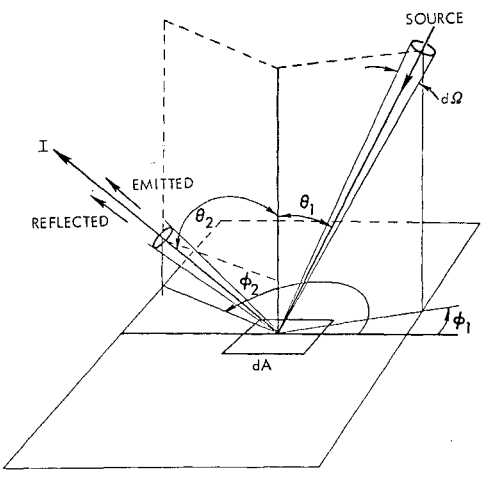

Fig. 1 Geometry of radiation incident and departing from a differential area of a surface.

$= \rho/\pi$ (where ρ is the reflectance of the surface), and Eq. (5) becomes

$$\begin{vmatrix} P_x \\ P_y \\ P_z \end{vmatrix} = -\begin{vmatrix} \sin\theta_0 \cos\varphi_0 \\ \sin\theta_0 \sin\varphi_0 \\ \cos\theta_0 \end{vmatrix} \left(\frac{G}{c}\right) \cos\theta_0 - \int_0^\infty \begin{vmatrix} 0 \\ 0 \\ \frac{2}{3} \end{vmatrix} \times \left(\frac{\rho_\lambda G_\lambda}{c}\right) \cos\theta_0 d\lambda - \int_0^\infty \begin{vmatrix} 0 \\ 0 \\ \frac{2}{3} \end{vmatrix} \epsilon(\lambda) \left[\pi I_B\left(\frac{T\lambda}{c}\right)\right] d\lambda \quad (6)$$

For a perfectly specular sample, the quantity f in Eq. (2) is a delta function so that

$$I^+(\theta_2, \varphi_2, \lambda) = \epsilon(\theta_2, \varphi_2, \lambda) I_b + \rho(\theta_1, \varphi_1, \lambda) I^- \qquad \theta_2 = \theta_1 \qquad \varphi_2 = \varphi_1 + \pi \quad (7)$$

In this case the stress Eq. (5), with $\rho = \rho(\theta_0, \varphi_0)$ averaged over the spectrum corresponding to G, becomes

$$\begin{vmatrix} P_x \\ P_y \\ P_z \end{vmatrix} = -\begin{vmatrix} \sin\theta_0 \cos\varphi_0(1-\rho) \\ \sin\theta_0 \sin\varphi_0(1-\rho) \\ \cos\theta_0(1+\rho) \end{vmatrix} \left(\frac{G}{c}\right) \cos\theta_0 - \int_0^\infty \int_0^{2\pi} \int_0^{\pi/2} \begin{vmatrix} \sin\theta_2 \cos\varphi_2 \\ \sin\theta_2 \sin\varphi_2 \\ \cos\theta_2 \end{vmatrix} \epsilon(\theta_2, \varphi_2, \lambda) \times \left[I_b\left(\frac{T\lambda}{c}\right)\right] \sin\theta_2 \cos\theta_2 d\theta_2 d\varphi_2 d\lambda \quad (8)$$

Equation (3) gives the general case, whereas Eqs. (6) and (8) are special cases for directional irradiation and diffuse and specular reflection, respectively. A final observation that may be made is that, if a maximum solar radiation moment is desired at a grazing angle of incidence, $\theta_0 \simeq 80°$–$90°$, as on a solar rudder sail, a diffuse reflecting surface is more desirable than a specular surface, and the best surface would be a grating blazed such that I^+ was directed along $\theta_2 = 0$. Such a grating could be made by embossing thin foil, for example.

References

[1] Clancy, T. F. and Mitchell, T. P., "Effect of radiation forces on the attitude of an artificial earth satellite," AIAA J. 2, 517 (1964).

[2] Polyakhova, Y. N., "Solar radiation pressure and the motion of earth satellites," AIAA J. 1, 2893 (1963).

[3] Holl, H. B., "The effect of radiation force on satellites of convex shapes," NASA TN D-604 (May 1961).

[4] McNicholas, H. J., "Absolute methods of reflectometry," J. Res. Natl. Bur. Std. 1, 29 (1928).

[5] Edwards, D. K. and Bevans, J. T., "Thermal radiation characteristics of imperfectly diffuse samples," TRW Space Technology Labs. Rept. 9990-6343-TU-000.

An Experimental Investigation of the Erosive Burning Characteristics of a Nonhomogeneous Solid Propellant

M. J. Zucrow,* J. R. Osborn,† and J. M. Murphy‡
Purdue University, Lafayette, Ind.

Nomenclature

A_{th} = area of the throat of the exhaust nozzle
A_{ts} = port area of the test section
g = acceleration due to gravity
k = ratio of specific heats of the combustion gases
M_{ts} = average Mach number of the combustion gases in the test section
O/F = ratio of the oxidizer to the binder by % wt
p_c = combustion pressure, psia
r_0 = linear burning rate
r = total burning rate, in./sec
r_e = erosive burning rate $(r - r_0)$
R = gas constant
SF = scale factor defined by Eq. (1)
t_i = propellant temperature; i.e., its temperature prior to ignition
t_f = flame temperature of the combustion gases
u_g = average velocity of the combustion gases, fps
u_{tv} = threshold velocity of the combustion gases; velocity above which $r > r_0$
Δt_b = burning time
Δx = change in the position of the burning surface during Δt_b

I. Introduction

In general, the burning rate of a solid propellant, denoted by r, is a complex function of many variables and may be represented by the following functional relation[1]:

$$r = r(p_c, t_f, t_i, u_g, O/F)$$

In addition, it is a function of the composition of the propellant, the oxidizer particle size (in a composite propellant), and the geometry of the propellant grain.

II. Experimental Investigation

The experiments were conducted with two-dimensional rocket motors comprising a gas generator and a test section; the propellant sample was burned in a two-dimensional test section.

Figure 1 illustrates the essential features of the test section; the propellant samples were bonded to its diverging sides. The divergence of the latter was such that the axial velocity of the combustion gases (discharged from the gas generator) was substantially constant in the region where they wetted the propellant samples.

In each experiment, the propellant sample burned in the test section was taken from the same bath of propellant that was burned in the gas generator. Consequently, there was no significant difference in the composition of the gases pro-

Presented as Preprint 64-107 at the AIAA Solid Propellant Rocket Conference, Palo Alto, Calif., January 29–31, 1964; revision received November 2, 1964. The research was sponsored by the Air Force Systems Command, Edwards Air Force Base, Calif., under Contract AF 04(611)-7445. Reproduction in whole or part is permitted for any purpose of the United States government. The authors express their thanks to the following individuals who were helpful in either conducting the research or preparing the paper: R. J. Burick, S. Lowe, W. Bloyd, and H. M. Cassiday.

* Atkins Professor of Engineering. Fellow Member AIAA.

† Professor of Mechanical Engineering. Associate Fellow Member AIAA.

‡ Research Assistant, Jet Propulsion Center; now Senior Engineer, Thiokol Chemical Corporation, Huntsville, Ala. Member AIAA.

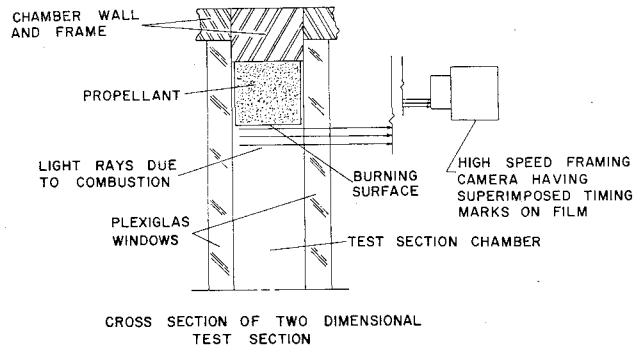

Fig. 1 Schematic diagram of photographic method for determining the burning rate of a solid propellant sample.

duced by the gas generator and those wetting the surface of the burning propellant sample located in the test section.

The test section was equipped with transparent Plexiglas (Rohm and Haas) windows so that light could be transmitted through the combustion chamber. A sample of the propellant to be investigated was mounted on the upper surface, and another sample was mounted on the lower surface of the test section; each sample was in the form of a parallelepiped block 5 in. long, 1 in. wide, and $\frac{1}{2}$ in. thick. The sides of the upper propellant sample were visible through the forementioned windows.

Only the upper sample was photographed during the burning period; a 16-mm Fastax (model WF3) high-speed framing camera was employed for that purpose. The camera, which was equipped with a Wollensak 152-mm f/4.5 cine telephoto lens, had a field of view approximately 1.5 in. in diameter. The camera was located with its optical axis normal to the plane of the transparent window. The average speed of the camera was approximately 720 frames/sec, and the speed was adjusted for each static firing of the research rocket motor; the aperture setting was f/32. All of the photographs were taken with Ansco Type 229 (color) film. A time base on the film was provided by a small argon lamp flashing at 120 cps.[2]

The combustion chamber pressure measurements were made by conventional electrical pressure transducers (Wiancko P 1951) and an oscillograph (Consolidated Electrodynamics Corporation Type 5-114-P4). The photographic record and the pressure traces recorded by the oscillograph were synchronized by employing separate event markers for

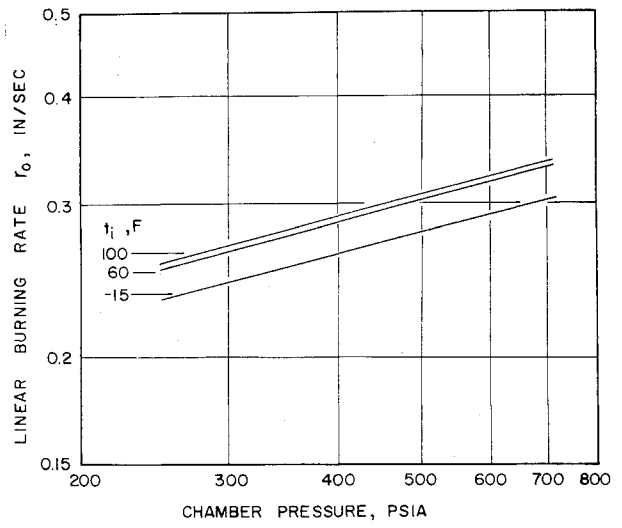

Fig. 2 Effect of combustion pressure and propellant temperature upon the linear burning rate of a solid propellant ($u_g = 0$).

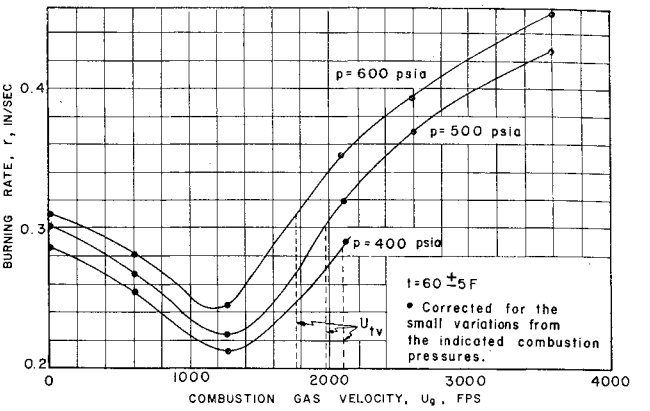

Fig. 3 Effect of combustion gas velocity and combustion pressure on the total burning rate of a solid propellant.

recording the activation of the igniter circuit. In this way, the burning rate of the propellant sample and its true combustion pressure were coordinated. Details of the instrumentation are presented in Refs. 3 and 4.

Calculations of burning rate from experimental data

The burning rate r of a propellant sample was calculated from the recession of the burning surface determined from the high speed photographs of its combustion. The burning rate was calculated by means of the following equation.[2] Thus

$$r = (SF)\Delta x/\Delta t_b \tag{1}$$

The average Mach number of the combustion gases in the test section M_{ts} was calculated from the equation[1]

$$\frac{A_{ts}}{A_{th}} = \frac{1}{M_{ts}}\left\{\frac{1 + [(k-1)/2]M_{ts}^2}{(k+1)/2}\right\}^{(k+1)/2(k-1)} \tag{2}$$

The average velocity of the combustion gases in the test section u_g was determined from the equation[1]

$$u_g = M_{ts}(kgRt_f)^{1/2}[1 + (k-1)/2M_{ts}^2]^{-1/2} \tag{3}$$

The calculated values of the burning rate were then plotted either as a function of the combustion chamber pressure and/or the combustion gas velocity past the burning surface of the propellant.

During an experiment, the following parameters were held constant: 1) the composition of the combustion gases, 2) the combustion pressure p_c, and 3) the propellant temperature t_i. The following variables were measured: 1) the static pressure at the fore-end of the gas generator, 2) the static pressures at the entrance and the exit sections of the test section, and 3) the burning rate r of the propellant sample located in the test section.

III. Experimental Results

Linear burning rate

The linear burning rate r_0 for the subject propellant was determined by burning a propellant sample, with no flow of combustion gas wetting the burning surface, in a small two-dimensional rocket motor employing the photographic technique described previously.

Table 1 Range of parameters

Parameter	Range of variation
Combustion pressure	400–600 psia
Velocity of the combustion gases	600–3600 fps
Initial temperature	$60 \pm 5F$

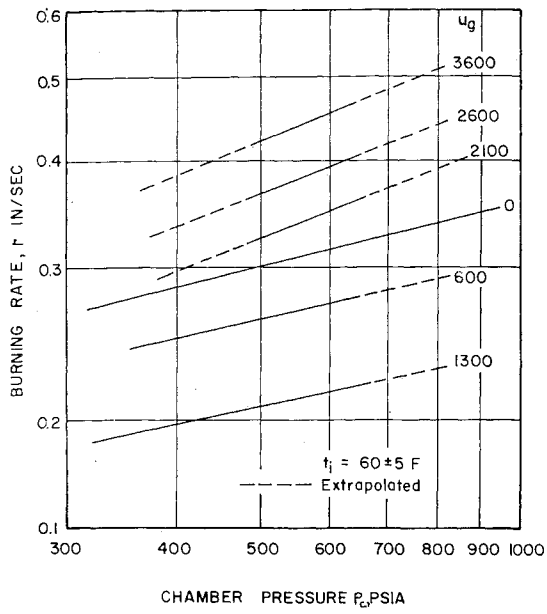

Fig. 4 Burning rate of a solid propellant as a function of chamber pressure with the combustion gas velocity as a parameter.

Figure 2 presents r_0, as a function of p_c for $t_i = -15 \pm 5F$, $60 \pm 5F$, and $100 \pm 5F$. All measurements were made at the same location from the fore-end of the propellant sample.

The values of r_0 determined with the research apparatus differed from those obtained from large rocket motor firings by less than 1%. The burning rates measured with the apparatus, at a given operating condition, were repetitive to within 3%. A minimum of three experiments were conducted at each operating point.[4, 5]

Combustion gas velocity

Table 1 presents the ranges over which u_g and p_c were varied during the investigation. Figure 3 presents the total burning rate r as a function of the combustion gas velocity u_g for the following constant values of combustion pressure: $p_c = 400$, 500, and 600 psia. The values of r measured at a given operating condition were repetitive to within 4%. At each operating point, a minimum of two to four runs were conducted. The curves indicate that for the particular propellant there is a "threshold" velocity u_{tv} above which the observed burning rate r is faster than the linear burning rate r_0; Fig. 3 shows that u_{tv} is a function of p_c.

Figure 4 presents the log$r$ as a function of the logp_c for the following constant values of u_g: 0, 600, 1300, 2100, 2600, and 3600 fps. The curve for $u_g = 0$ corresponds to the linear burning rate r_0 obtained at a propellant temperature $t_i = 60 \pm 5F$.

Propellant temperature

Experiments were conducted for determining the influence of the propellant temperature t_i upon the burning rate r; the latter includes the contribution due to erosive burning. Two different values of propellant temperature were investigated: $t_i = -15 \pm 5$ and $t_i = 100 \pm 5F$. Table 2 presents the results obtained from experiments for determining the influence of t_i.

The data presented in Table 2 indicate that the erosive burning rate r_e is influenced by the initial temperature of the propellant t_i and increases as t_i decreases.

IV. Conclusions

Based on the experiments discussed in this paper, the following conclusions, pertinent to the subject propellant, may be drawn: 1) the photographic technique permits determining the instantaneous (less than 0.1 sec) burning rate r of a solid propellant sample; 2) under erosive burning conditions, the subject solid propellant exhibits a threshold velocity, which is pressure dependent; 3) limited experiments indicate that a decrease in the propellant temperature t_i produces an increase in the erosive burning rate r_e of the propellant.

Table 2 Comparison of burning rates as a function of initial temperature (t_i)

Parameter	$-15F$	$60F$	$60F$	$100F$
Combustion pressure, psia	535	547	652	620
Velocity of the combustion gases, fps	2460	2560	3140	3180
Total burning rate r, in./sec	0.38	0.37	0.42	0.36
Linear burning rate r_0, in./sec	0.28	0.31	0.33	0.32
Erosive burning rate r_e, in./sec	0.10	0.06	0.09	0.04

References

[1] Zucrow, M. J., *Aircraft and Missile Propulsion* (John Wiley and Sons, Inc., New York, 1958), Vol. 2, Chap. 10.

[2] Osborn, J. R., Murphy, J. M., and Kershner, S. D., "Photographic measurement of burning rates in solid propellant rocket motors," Rev. Sci. Instr. **34**, 305–306 (1963).

[3] Murphy, J. M. and Bethel, H. E., "Investigation of new techniques for measuring the burning rate of a solid rocket propellant," Jet Propulsion Center, Purdue Univ. TM-62-8 (October 1962); confidential.

[4] Zucrow, M. J., Osborn, J. R., Murphy, J. M., and Kershner, S. D., "Final report on the investigation of velocity upon burning rate of solid propellants," Jet Propulsion Center, Purdue Univ. Rept. F-63-3 (December 1963); confidential.

[5] Zucrow, M. J., Osborn, J. R., and Murphy, J. M., "The erosive burning of a non-homogeneous solid propellant," 56th Annual AIChE Meeting (December 1963).

Characteristics of Supersonic Ejector Systems with Nonconstant Area Shroud

W. L. Chow* and P. S. Yeh†
University of Illinois, Urbana, Ill.

In our recent studies of supersonic ejector systems,[1, 2] a flow model has been developed stressing the detailed inviscid and viscid interaction between the primary and the secondary streams. The flow phenomena associated with various flow regimes were described and analyzed. The theoretical results thus calculated for ejector systems with cylindrical constant area shrouds were in excellent agreement with those obtained from experiments. This analysis has also been applied to study the starting characteristics of ejector systems.[3] It is intended here to show the applicability of this method to ejector systems with nonconstant area shrouds. The theoretical calculations are only carried out for the "supersonic regime" of the system where the ambient pressure ratio P_a/P_{op} is kept at such low level that it will exert no influence on the flows at the upstream. For the purpose of comparison, experimental results are also obtained for the calculated ejector systems.

Received August 21, 1964. This work was partially supported by NASA as part of a broad research program under Research Grant NsG-13-59. The authors are grateful to H. H. Korst for his continued interest in this problem, and to A. L. Addy for his help in the experimental investigations.

* Associate Professor of Mechanical Engineering. Member AIAA.

† Graduate Research Assistant.